

Synchrotron Mössbauer spectroscopic and x-ray diffraction study of ferropericlase in the high-pressure range of the lower mantle region

Maki Hamada,^{1,*} Seiji Kamada^{1,2}, Eiji Ohtani¹, Tatsuya Sakamaki¹, Takaya Mitsui³, Ryo Masuda⁴, Naohisa Hirao⁵, Yasuo Ohishi⁵, and Masahide Akasaka⁶

¹Department of Earth Science, Graduate School of Science, Tohoku University, Sendai 980-8578, Japan

²Frontier Research Institute for Interdisciplinary Sciences, Tohoku University, Sendai 980-8578, Japan

³National Institutes for Quantum and Radiological Science and Technology, 1-1-1, Kouto, Sayo, Hyogo 679-5148, Japan

⁴Research Reactor Institute, Kyoto University, Asashironishi, Kumatori, Sennan, Osaka 590-0494, Japan

⁵Japan Synchrotron Radiation Research Institute, Sayo, Hyogo 679-5198, Japan

⁶Department of Geoscience, Graduate School of Science and Engineering, Shimane University, Matsue 690-8504, Japan



(Received 22 February 2021; accepted 15 April 2021; published 12 May 2021)

Systematic change of structural transition and high-spin (HS) to low-spin (LS) transition of Fe²⁺ in synthetic (Mg_{0.6}Fe_{0.4})O-ferropericlase for pressures up to that of the lower mantle region were investigated using synchrotron x-ray diffraction (XRD) and synchrotron Mössbauer spectroscopic methods. The XRD patterns and the Mössbauer spectra were measured up to 160 GPa at room temperature. The results of the synchrotron XRD analysis indicate that the cubic structure of (Mg_{0.6}Fe_{0.4})O-ferropericlase is maintained up to 160 GPa. The Mössbauer spectra at 19.8 and 24.0 GPa consist of three doublets assigned to HS Fe²⁺ at the octahedral site. At pressures from 61 to 136 GPa, a singlet assigned to LS Fe²⁺ is added to the three HS Fe²⁺ doublets, and its area ratio with respect to the HS Fe²⁺ doublets gradually increase with increasing pressure. At pressures above 136 GPa, the Mössbauer spectra consist of only an LS Fe²⁺ singlet, implying that all Fe at these pressures is in a LS state. The resulting spin crossover pressure interval from 61 to 136 GPa indicates the coexistence of both HS and LS Fe²⁺ at pressure conditions from the upper part to the bottom of the lower mantle.

DOI: [10.1103/PhysRevB.103.174108](https://doi.org/10.1103/PhysRevB.103.174108)

I. INTRODUCTION

(Mg_{1-x}Fe_x)O minerals (periclase with $x < 0.5$; wüstite with $x > 0.5$) are considered to be one of the main phases of the Earth's lower mantle [1–7]. Since Fe-bearing periclase with a composition between $x = 0.1$ and 0.4 (hereinafter, referred to as ferropericlase) is expected to be the second-most-abundant mineral of the Earth's lower mantle after (Mg, Fe)SiO₃ phase, this mineral has been studied using the synchrotron x-ray diffraction (XRD) method, x-ray emission spectroscopy, Mössbauer spectroscopy, and x-ray absorption near-edge structure analysis (XANES) to clarify its structural transition and the spin transition of Fe²⁺ at high pressures [1–10]. Moreover, the FeO end member wüstite at high pressures has been studied in detail to understand its structural transition, the spin transition of Fe²⁺, and its magnetic properties [5,11–15].

Ferropericlase and wüstite have a cubic structure with space group $Fm\bar{3}m$ (B1 in Strukturbericht designation) at ambient pressure and temperature and transform into a rhombohedral structure with space group $R\bar{3}m$ at high pressure. The transition pressure depends on the chemical composition of periclase-wüstite solid solution. The structural transition for wüstite takes place at pressure >9–18GPa at

300 K for wüstite [5,16–19] and at a pressure >20 GPa for (Mg_{0.10}Fe_{0.90})O-wüstite [3]. However, as noted by Kantor [20], some controversy exists regarding the minimum iron content that allows structural transition in ferropericlase. Lin *et al.* [21] reported that no structural transition occurs in (Mg_{0.39}Fe_{0.61})O-wüstite up to 102 GPa, whereas *in situ* experiments combining the XRD method, Mössbauer spectroscopy, and XANES spectroscopy under nonhydrostatic stress conditions revealed the structural transition of (Mg_{0.80}Fe_{0.20})O-ferropericlase with a cubic system to the phase with a trigonal system at 35(1) GPa and room temperature and determined the unit-cell parameters of the trigonal (Mg_{0.8}Fe_{0.2})O-ferropericlase at 41 GPa as $a = 2.810(5)$ Å and $\alpha = 60.70(1)^\circ$ [7]. Based on their results and published data, Kantor *et al.* [7] constructed a phase diagram for (Mg,Fe)O phase at room temperature showing the phase boundary on the structural transition from B1 to trigonal systems, in which the B1-to-trigonal transition boundary obtained by nonhydrostatic stress experiments is located on the lower-pressure side than that obtained by hydrostatic stress experiments. The result by Speziale *et al.* [3] that (Mg_{0.8}Fe_{0.2})O-ferropericlase remains a B1 structure, at least up to 62 GPa under hydrostatic conditions, is consistent with the suggestion by Kantor *et al.* [7] that the transition from a cubic system to a trigonal system could be stress induced.

A further structural transition of wüstite from a trigonal structure to a hexagonal structure with space group $P6_3/mmc$ (B8 in Strukturbericht designation) at ~ 70 –75 GPa and 600–1600 K has also been proposed [22–27]. The transition

*hamada.m@staff.kanazawa-u.ac.jp

†Present address: School of Geoscience and Civil Engineering, College of Science and Engineering, Kanazawa University, Kanazawa 920-1192, Japan.

from a B1 structure to a B8 structure, observed in wüstite, did not occur in ferropericlase and Mg-bearing wüstite under hydrostatic stress conditions up to 86–102 GPa and 2500 K [21,24].

Although structural transitions from B1 to distorted structures with lower symmetries in transition metal monoxides were suggested to be due to the exchange interactions that result from antiferromagnetic ordering [28], high-pressure Mössbauer and ultrasonic elasticity study of wüstite revealed a magnetic transition at ~ 5 GPa, which differs significantly from the structural transition pressure [4,5]. Moreover, Kantor *et al.* [7] indicated that, despite a structural transition in $(\text{Mg}_{0.8}\text{Fe}_{0.2})\text{O}$ -ferropericlase at 35(1) GPa and room temperature, magnetic splitting was not recognized in the Mössbauer data of the high-pressure phase (≥ 56 GPa), which proves the stability of the rhombohedral distortion in the absence of magnetic ordering. Therefore, Kantor *et al.* [7] concluded that a rhombohedral distortion of $(\text{Mg}_{0.8}\text{Fe}_{0.2})\text{O}$ -ferropericlase is not associated with long-range magnetic ordering.

As reviewed by Speziale *et al.* [3] for the experimental and theoretical results on the periclase-wüstite solid solution, the pressure at which the high-spin (HS) to low-spin (LS) transition in Fe^{2+} ions takes place increases with increasing FeO content in periclase-wüstite solid solution: 40–60 GPa for ferropericlase with 10 mol.% FeO, and > 80 –90 GPa for Mg-bearing wüstite and wüstite [2,6–9,12,29–33]. In Mössbauer spectroscopy and x-ray emission spectroscopic studies for $(\text{Mg}_{0.8}\text{Fe}_{0.2})\text{O}$ -ferropericlase by Kantor *et al.* [7], they assigned a Mössbauer doublet appearing $> \sim 50$ GPa to Fe^{2+} in the LS state and showed that the spin crossover pressure at room temperature ranges until just > 100 GPa, based on the calculated spin number and the relative area ratio of the LS Fe^{2+} doublet. On the other hand, Hamada *et al.* [15] performed a Mössbauer study of synthetic $\text{Fe}_{0.96}\text{O}$ -wüstite at pressures up to 203 GPa at 300 K using synchrotron Mössbauer spectroscopy and found that the magnetic component of Fe^{2+} decreases gradually with increasing pressure from 91 to 203 GPa, while the nonmagnetic component increases with pressure in the same pressure range.

In addition to studies focused on wüstite and ferropericlase with rather poor Fe content, Fei *et al.* [34] measured simultaneous high P - T synchrotron XRD data of $(\text{Mg}_{0.6}\text{Fe}_{0.4})\text{O}$ -ferropericlase to 30 GPa and 800 K, because the ferropericlase with 40 mol.% FeO is in equilibrium with perovskite with 10 mol.% Fe under lower mantle conditions [34], and applied the experimental P - V - T data to derive geophysically relevant parameters, such as bulk modulus, the Anderson-Grüneisen parameter, and the Grüneisen parameter. Recently, Solomatova *et al.* [35] indicated that the spin crossover range of $(\text{Mg}_{0.52}\text{Fe}_{0.48})\text{O}$ -ferropericlase is from 44 to 84 GPa by XRD and time-domain synchrotron nuclear forward scattering analysis and suggested that the spin crossover might have been completed > 84 GPa.

In this paper, synthetic $(\text{Mg}_{0.6}\text{Fe}_{0.4})\text{O}$ -ferropericlase was investigated using energy-domain Mössbauer absorption spectroscopy at 19.8, 24.0, 61, 97, 108, 120, 130, 136, and 160 GPa and synchrotron XRD methods at 19.8, 24.0, 35.7, 61, 103.0, 120, 130, 136, 153, and 160 GPa to clarify the systematic change of structural transition and

spin state transition of Fe^{2+} against the Fe^{2+} content in ferropericlase.

II. EXPERIMENTAL METHODS

A. Synthesis of $(\text{Mg}_{0.6}\text{Fe}_{0.4})\text{O}$ -ferropericlase used for high-pressure experiments

Ferropericlase with a composition of $(\text{Mg}_{0.6}\text{Fe}_{0.4})\text{O}$ used as a starting material was synthesized by sintering of a mixture of $^{57}\text{Fe}_2\text{O}_3$ (96.63% of ^{57}Fe enrichment, ISOFLEX) and MgO (99.0%, Junsei Chemical Co., Ltd.) at low oxygen fugacity. The mixture was pressed into thin pellets and placed in a platinum crucible. The mixture was held at 1400 °C for 34 h at an oxygen fugacity condition higher than that of the iron-wüstite buffer, which was obtained by controlling the H_2 - CO_2 gas mixture [36]. Finally, the sample was quenched at liquid nitrogen temperature.

To determine the phase and lattice constant, the synthetic product of $(\text{Mg}_{0.6}\text{Fe}_{0.4})\text{O}$ -ferropericlase was identified using powder XRD by $\text{Cu K}\alpha$ radiation at room temperature. The powdered product was formed into a pellet and mounted on a silicon plate. Step-scan powder diffraction data were collected using a Bruker D8 ADVANCE automated Bragg-Brentano diffractometer system equipped with incident- and diffracted-beam Soller slits, 1° divergence and scatter slits, a 0.15 mm receiving slit, and a LINXEYE detector. The Cu x-ray tube was operated at 40 kV and 40 mA. Profiles were taken between 20° and 80° 2θ using a step interval of 0.02° and a step counting time of 2.0 s. The XRD profiles were analyzed by PDIndexer [37,38] using a Symmetric Pseudo-Voigt function. The XRD pattern of this product at ambient conditions (Fig. 1) indicates a single phase of ferropericlase of the cubic system with space group $Fm\bar{3}m$. The lattice constant was determined to be $a = 4.260(1)$ Å, which is consistent with the result on the $(\text{Mg}_{0.6}\text{Fe}_{0.4})\text{O}$ ferropericlase by Rosenhauer *et al.* [39] and Solomatova *et al.* [35]. Thus, we conclude that the synthetic product is a single phase with the $(\text{Mg}_{0.6}\text{Fe}_{0.4})\text{O}$ -ferropericlase.

The Mössbauer spectrum of the synthetic $(\text{Mg}_{0.6}\text{Fe}_{0.4})\text{O}$ -ferropericlase measured using the BL11XU beam line of the SPring-8 synchrotron radiation facility, Hyogo, Japan, in the ambient condition (details of the method are given below) is shown in Fig. 1. The spectrum was fitted with three nonmagnetic doublets: isomer shift (IS) = 1.07(2) and quadrupole splitting (QS) = 0.3(2) mm/s for doublet AA', IS = 1.12(2) and QS = 1.0(2) mm/s for the doublet BB', and IS = 1.07(2) and QS = 1.6(2) mm/s for the doublet CC' (Table I). These values, especially IS values, indicate that all the doublets are assigned to be HS Fe^{2+} at the octahedral sites.

B. Synchrotron XRD and synchrotron Mössbauer spectroscopic analyses at high pressure

The experiments at room temperature and high pressure were performed using a diamond anvil cell with culet sizes of 75, 200, and 300 μm . A rhenium or tungsten metal sheet was pre-indented to 20 μm in thickness. The holes drilled into the gasket as a sample chamber for each culet size were 20–28 μm in thickness (t) \times ϕ 18–30 μm for a culet size of 75 μm , $t = 32 \times \phi$ 100 μm for a culet size of 200 μm , and

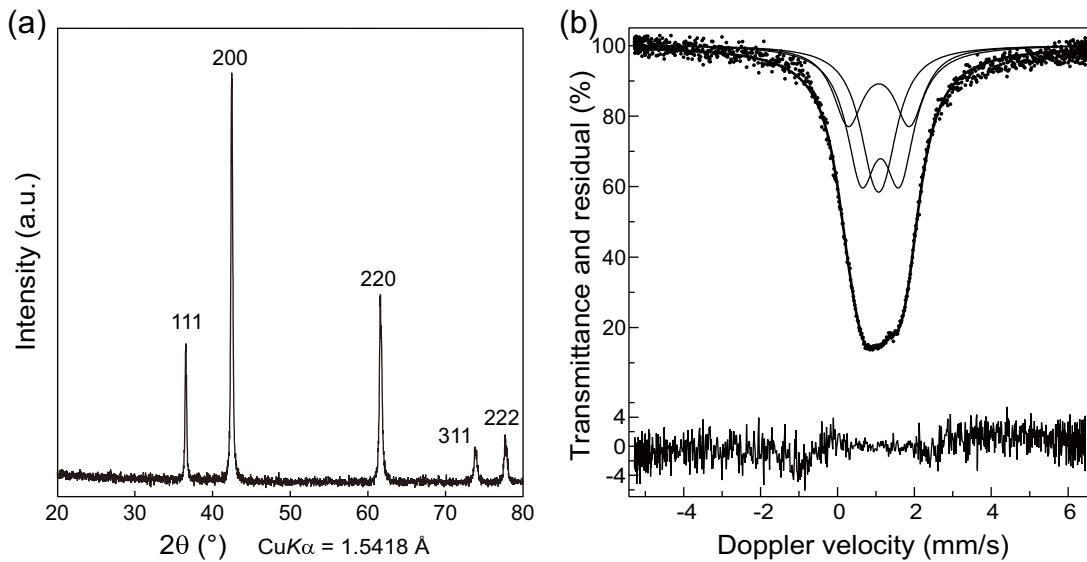


FIG. 1. (a) X-ray diffraction pattern measured using a Bruker D8 ADVANCE and (b) Mössbauer spectrum measured at SPring-8 BL11XU of $(\text{Mg}_{0.6}\text{Fe}_{0.4})$ -ferropericlasite at 1 atm. The residual is shown below the spectrum. The doublets are least-square fits to the empirical data assuming quadrupole split components with different intensities.

$t = 57 \times \phi 120 \mu\text{m}$ for a culet size of $300 \mu\text{m}$. Potassium chloride (KCl), heated for 2 h for the purpose of desiccation, was used as the pressure medium for experiments at 130, 136, 153, and 160 GPa, and potassium bromide (KBr), heated for 2 h for the purpose of desiccation, was used as the pressure medium for experiments at 0, 24, 35.7, and 103.0 GPa. The experiments at 19.8, 61, 97, 108, and 120 GPa were performed without pressure medium. The pressure was estimated by the ruby fluorescence method [40] and the diamond T_{2g} Raman shift [41].

Synchrotron XRD patterns at 19.8, 24.0, 35.7, 61, 103.0, 120, 130, 136, 153, and 160 GPa and room temperature were measured at the BL10XU beamline of the SPring-8 [42] synchrotron radiation facility, Harima, Japan. A pinhole with a diameter of $50 \mu\text{m}$ and an imaging plate detector (Rigaku R-AxisIV⁺⁺, $300 \times 300 \text{ mm}$, pixel size: 0.10 mm) were used. The measured two-dimensional images were analyzed by the IPAnalyzer software package, and one-dimensional profiles were analyzed by the PDIndexer software package [37,38].

The ^{57}Fe -Mössbauer spectra measurements in the energy domain using a nuclear Bragg monochromator were performed at 19.8, 24.0, 61, 97, 108, and 120 GPa at the BL11XU beamline and at 130, 136, and 160 GPa at the BL10XU beamline [43,44]. The energy for the γ rays used in the synchrotron Mössbauer spectroscopic experiments was 14.4125 keV, which was obtained from x-rays using a double-crystal premonochromator. Then the bandwidth of the incident x-ray was set to be $\sim 2.5\text{--}4 \text{ meV}$ using a high-resolution monochromator (HRM). The HRM was placed in front of the sample at the BL11XU and behind the sample at the BL10XU to take XRD patterns. The incident x-ray beam was monochromatized to a single line by a $^{57}\text{FeBO}_3$ single crystal near the Néel temperature in the magnetic field. The final energy bandwidth of the x-ray beam was set to be $15\text{--}16 \text{ neV}$. The source Doppler shift was obtained by oscillating the crystal parallel to the reflection plane [43,44]. The size of the incident beam

in the experimental hatch was $0.4(V) \times 1.6(H) \text{ mm}$, and the beam was horizontally focused to $0.4(V) \times 0.02(H) \text{ mm}$ in size at the BL11XU and $0.05(V) \times 0.15(H) \text{ mm}$ in size at the BL10XU. The Mössbauer data were counted using a NaI scintillation counter and were obtained using a sinusoidal acceleration spectrometer fitted with a 1024-channel analyzer. The typical data collection time range was from 1 to 9 h for spectra, depending on the pressure. The IS was referenced to a standard metallic ^{57}Fe foil at room temperature under ambient pressure, and the Doppler velocity was calibrated with respect to the same standard. The MossA software package [45] was used for computational analysis.

III. RESULTS

A. Synchrotron XRD analysis of the $(\text{Mg}_{0.6}\text{Fe}_{0.4})\text{O}$ -ferropericlasite at high pressure

The synchrotron XRD patterns of the $(\text{Mg}_{0.6}\text{Fe}_{0.4})\text{O}$ -ferropericlasite measured up to 160 GPa are shown in Fig. 2. The XRD patterns at 19.8, 24.0, and 35.7 GPa indicate that the $(\text{Mg}_{0.6}\text{Fe}_{0.4})\text{O}$ -ferropericlasite has a cubic B1 structure. At pressures $> 61 \text{ GPa}$, the broadening of the Bragg reflections with 111, 220, 311, and 222 indices in the cubic system is observed in the XRD patterns. In addition, the reflection with a 220 index splits slightly at 120 GPa. Kantor *et al.* [7] found such broadening of the Bragg reflection in the XRD profile of $(\text{Mg}_{0.8}\text{Fe}_{0.2})\text{O}$ -ferropericlasite at high pressure and revealed that the Bragg reflection broadening is due to the structural transformation of a B1 structure to a rhombohedral structure. The broadened 111, 220, 311, and 222 reflections based on the B1 structure are in fact the overlapped reflections of $011 + 111$, $\bar{1}01 + 112$, $\bar{1}\bar{1}1 + 012 + 122$, and $220 + 222$ in the rhombohedral structure. In contrast to the case of $(\text{Mg}_{0.8}\text{Fe}_{0.2})\text{O}$ -ferropericlasite, the broadening of the Bragg reflection for $(\text{Mg}_{0.6}\text{Fe}_{0.4})\text{O}$ -ferropericlasite in

TABLE I. Mössbauer hyperfine parameters of synthetic ferroperricite.

Beamline	Pressure	Pressure medium	Doublets	IS ^a (mm/s)	QS ^b (mm/s)	Γ^c (mm/s)	Area ratio (%)	Assignment	
BL11XU	Ambient condition	KBr	Three doublets						
			AA'	1.07(2)	0.3(2)	0.94(4)	29(10)	Fe ²⁺ (HS)	
			BB'	1.12(2)	1.0(2)	0.94(4)	44(11)	Fe ²⁺ (HS)	
				CC'	1.07(2)	1.6(2)	0.94(4)	27(10)	Fe ²⁺ (HS)
	19.8(9)	No	Three doublets						
			AA'	0.898(4)	0.43(3)	0.82(2)	33(1)	Fe ²⁺ (HS)	
			BB'	0.925(4)	1.30(4)	0.82(3)	40(1)	Fe ²⁺ (HS)	
				CC'	0.907(6)	2.11(4)	0.82(4)	27(1)	Fe ²⁺ (HS)
	24.0(9)	KBr	Three doublets						
			AA'	0.895(7)	0.41(3)	0.78(2)	33(2)	Fe ²⁺ (HS)	
			BB'	0.951(5)	1.72(4)	0.78(3)	45(2)	Fe ²⁺ (HS)	
				CC'	0.90(1)	2.09(5)	0.78(4)	22(2)	Fe ²⁺ (HS)
	61(1)	No	Three doublets and singlet						
			AA'	0.823(3)	0.75(2)	0.66(2)	33(1)	Fe ²⁺ (HS)	
			BB'	0.834(3)	1.44(3)	0.66(2)	33(1)	Fe ²⁺ (HS)	
			CC'	0.807(6)	2.14(3)	0.66(2)	17.8(9)	Fe ²⁺ (HS)	
				D	0.808(4)		0.66(2)	15.9(7)	Fe ²⁺ (LS)
	97(1)	No	Three doublets and singlet						
			AA'	0.632(6)	0.70(6)	0.73(4)	37(2)	Fe ²⁺ (HS)	
			BB'	0.648(7)	1.42(6)	0.73(4)	31(2)	Fe ²⁺ (HS)	
			CC'	0.60(2)	2.24(7)	0.73(4)	13(1)	Fe ²⁺ (HS)	
				D	0.615(8)		0.73(4)	19(2)	Fe ²⁺ (LS)
	108(8)	No	Three doublets and singlet						
			AA'	0.592(6)	0.69(7)	0.72(5)	39(3)	Fe ²⁺ (HS)	
BB'			0.603(8)	1.38(9)	0.72(5)	28(3)	Fe ²⁺ (HS)		
CC'			0.57(2)	2.1(1)	0.72(5)	13(3)	Fe ²⁺ (HS)		
			D	0.579(8)		0.72(5)	19(3)	Fe ²⁺ (LS)	
120(7)	No	Three doublets and singlet							
		AA'	0.503(8)	0.79(9)	0.84(7)	42(3)	Fe ²⁺ (HS)		
		BB'	0.47(1)	1.6(1)	0.84(7)	25(3)	Fe ²⁺ (HS)		
		CC'	0.37(4)	2.3(2)	0.84(7)	9(3)	Fe ²⁺ (HS)		
			D	0.491(8)		0.84(7)	24(3)	Fe ²⁺ (LS)	
BL10XU	130(1)	KCl	Three doublets and singlet						
			AA'	0.63(4)	0.8(1)	0.7(2)	41(7)	Fe ²⁺ (HS)	
			BB'	0.76(8)	1.9(2)	0.7(2)	16(5)	Fe ²⁺ (HS)	
			CC'	1.0(2)	2.9(5)	0.7(2)	8(4)	Fe ²⁺ (HS)	
				D	0.54(3)		0.7(2)	36(7)	Fe ²⁺ (LS)
	136(1)	KCl	One singlet						
			D	0.59(2)		1.52(9)	100	Fe ²⁺ (LS)	
	160(1)	KCl	One singlet						
			D	0.49(3)		1.4(1)	100	Fe ²⁺ (LS)	

^aIsomer shift referenced to a metallic iron absorber.

^bQuadrupole splitting.

^cFull width at half maximum.

this paper is observed in all XRD patterns measured at high pressure, and there is no unique diffraction due to the trigonal structure. Thus, the Bragg reflection broadening of (Mg_{0.6}Fe_{0.4})O-ferroperricite at high pressure cannot be attributed to the cubic-rhombohedral structural transformation. We assume that the nonhydrostatic conditions in the sample chamber are the reason for the Bragg reflection broadening. In the experiments at 24, 35.7, 103.0, 130, 136, 153, and 160 GPa, KCl and KBr were used as pressure media to achieve the hydrostatic stress condition, although the experiments at 19.8, 61, 97, 108, and 120 GPa were performed without a pressure medium. However, Takemura [46] indicated that, even in the

high-pressure experiments using a pressure medium, the hydrostatic condition was not necessarily realized because the solid pressure-transmitting medium did not practically affect the achievement of the hydrostatic condition. Therefore, the broadening of XRD peaks may have been caused by microstrain and related stress under the nonhydrostatic condition.

To compare the obtained result with the data by Fei *et al.* [47] and that by Solomatova *et al.* [35], the cell volume of the (Mg_{0.6}Fe_{0.4})O-ferroperricite in this paper, calculated as the cubic system, is shown with respect to pressure in Fig. 3. The above studies also indicated that ferroperricites with chemical compositions like that of this paper preserve the cubic struc-

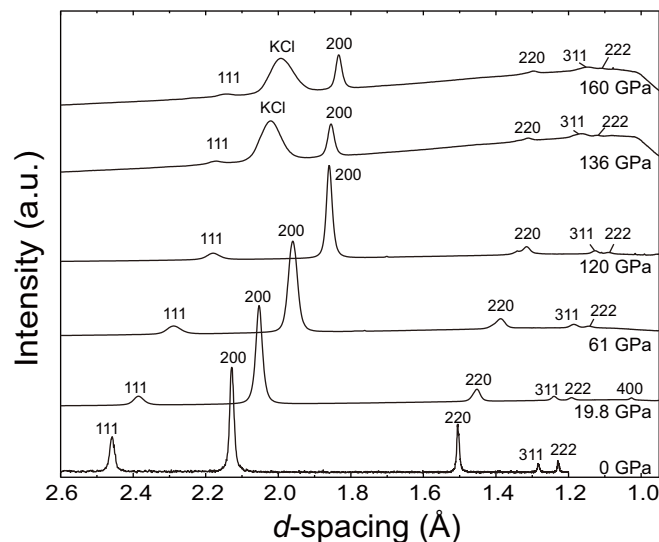


FIG. 2. X-ray diffraction patterns of $(\text{Mg}_{0.6}\text{Fe}^{2+}_{0.4})$ -ferropericlase measured at room temperature. Diffraction peaks with Miller indices belonging to $(\text{Mg}_{0.6}\text{Fe}^{2+}_{0.4})$ -ferropericlase. KCl: pressure medium. The diffraction pattern at 0 GPa is measured using a Bruker D8 ADVANCE.

ture up to 148 GPa [35,47]. Although Fei *et al.* [47] reported a volume change with pressure up to 140 GPa, the discontinuity at ~ 120 GPa has not been reported. Our result showed that the cell volume calculated as a cubic system becomes nearly constant at pressures between 120 and 136 GPa and decreases again at pressures from 136 to 160 GPa. This change is also recognized in the cell volume variation with respect to the pressure reported by Fei *et al.* [47].

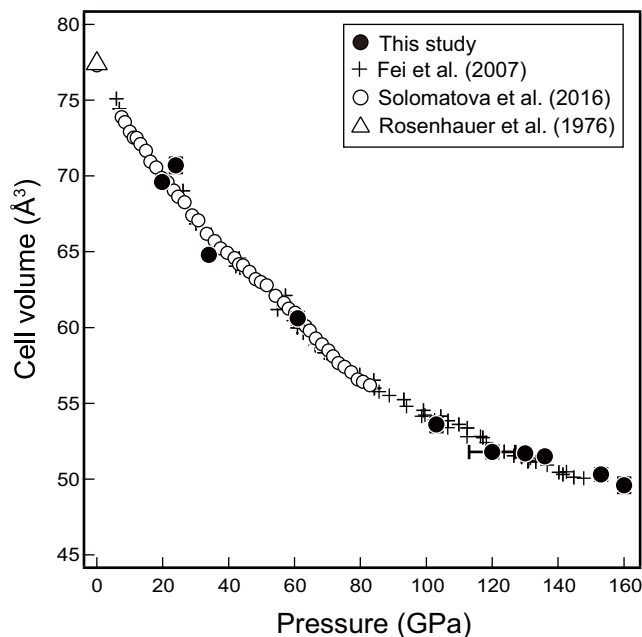


FIG. 3. Pressure-volume relationship of $(\text{Mg}_{0.6}\text{Fe}^{2+}_{0.4})$ -ferropericlase at room temperature.

B. Synchrotron Mössbauer spectroscopic analysis at high pressure

The Mössbauer spectra and fitted doublets and singlets are shown in Fig. 4. The Mössbauer hyperfine parameters at these pressures are shown in Table I. Based on the results reported by Kantor [20], the Mössbauer spectra of the $(\text{Mg}_{0.95}\text{Fe}_{0.05})\text{O}$ - and $(\text{Mg}_{0.8}\text{Fe}_{0.2})\text{O}$ -ferropericlase up to 41 and 43 GPa, respectively, consisted of one doublet. In contrast, the Mössbauer spectra of the $(\text{Mg}_{0.6}\text{Fe}_{0.4})\text{O}$ -ferropericlase at 19.8 and 24.0 GPa in this paper consist of three doublets with $\text{IS} = 0.895\text{--}0.898$ and $\text{QS} = 0.41\text{--}0.43$ mm/s, $\text{IS} = 0.925\text{--}0.951$ and $\text{QS} = 1.30\text{--}1.72$ mm/s, and $\text{IS} = 0.90\text{--}0.907$ and $\text{QS} = 2.11\text{--}2.09$ mm/s, which are assigned to HS Fe^{2+} in the octahedral site. Solomatova *et al.* [35] also detected two doublets assigned to HS Fe^{2+} at the octahedral site in their Mössbauer spectra of $(\text{Mg}_{0.52}\text{Fe}^{2+}_{0.48})\text{O}$ -ferropericlase measured at pressures from 4 to 37 GPa. These results indicate that the octahedral sites in the $(\text{Mg}_{0.6}\text{Fe}_{0.4})\text{O}$ -ferropericlase are locally distorted by three types of next-nearest-neighbor configurations of iron cations in the octahedral sites. The effect of next-nearest-neighbor configurations of iron cations at any cation site on the local distortion of the coordination polyhedra has also been recognized by Mössbauer spectroscopic studies on the Fe distribution at the octahedral sites in pyroxene [48] and at the tetrahedral sites in melilite [49,50].

In the Mössbauer spectra at 61–130 GPa (Fig. 4), a new component with virtually zero QS was fitted in addition to three doublets due to HS Fe^{2+} . This component, fitted with a singlet in this paper, shows smaller IS ($\text{IS} = 0.808(4)$ mm/s at 61 GPa to $0.491(8)$ mm/s at 120 GPa) than the main HS Fe^{2+} doublets AA' and BB' ($\text{IS} = \sim 0.807\text{--}0.834$ mm/s at 61 GPa to $0.37\text{--}0.503$ mm/s at 120 GPa). Kantor [20] also reported a component with zero QS and low IS in the Mössbauer spectra of $(\text{Mg}_{0.95}\text{Fe}_{0.05})\text{O}$ and $(\text{Mg}_{0.8}\text{Fe}_{0.2})\text{O}$ -ferropericlase measured $> \sim 50$ GPa and assigned this component to LS Fe^{2+} at the octahedral site. We agree to the assignment by Kantor [20], and thus, the singlet is assigned to LS Fe^{2+} in the $(\text{Mg}_{0.6}\text{Fe}_{0.4})\text{O}$ -ferropericlase. The Mössbauer spectrum at 130 GPa measured at the BL10XU beamline also consists of three doublets AA', BB', and CC' ($\text{IS} = 0.63\text{--}1.0$ mm/s) assigned to HS Fe^{2+} and a singlet D ($\text{IS} = 0.54$ mm/s) due to LS Fe^{2+} . However, the IS values of the doublets AA', BB', and CC' deviate from the trends of those measured at the BL11XU beamline at 61–120 GPa (Fig. 5). One reason for such a deviation of the data at 130 GPa may be attributed to low statistics by limited x-ray flux. The Mössbauer spectra at 136–160 GPa were fitted with one singlet assigned to LS Fe^{2+} in the octahedral site (Fig. 5), although the full widths at half maximum (FWHMs; $\Gamma = 1.52(9)$ and $1.4(1)$ mm/s at 136 and 160 GPa, respectively) are significantly larger than the singlet at 60–130 GPa ($\Gamma = \sim 0.66\text{--}0.84$ mm/s; Table I). The broadened FWHMs of $(\text{Mg}_{0.6}\text{Fe}_{0.4})\text{O}$ -ferropericlase may be caused by the overlap with the other doublet, which is attributed to HS Fe^{2+} .

Kantor *et al.* [7] found a linear decrease of the IS values of $(\text{Mg}_{0.8}\text{Fe}_{0.2})\text{O}$ -ferropericlase with increasing pressure up to 56 GPa. This paper clarified that the IS values of the main doublets assigned to HS Fe^{2+} decrease almost linearly with

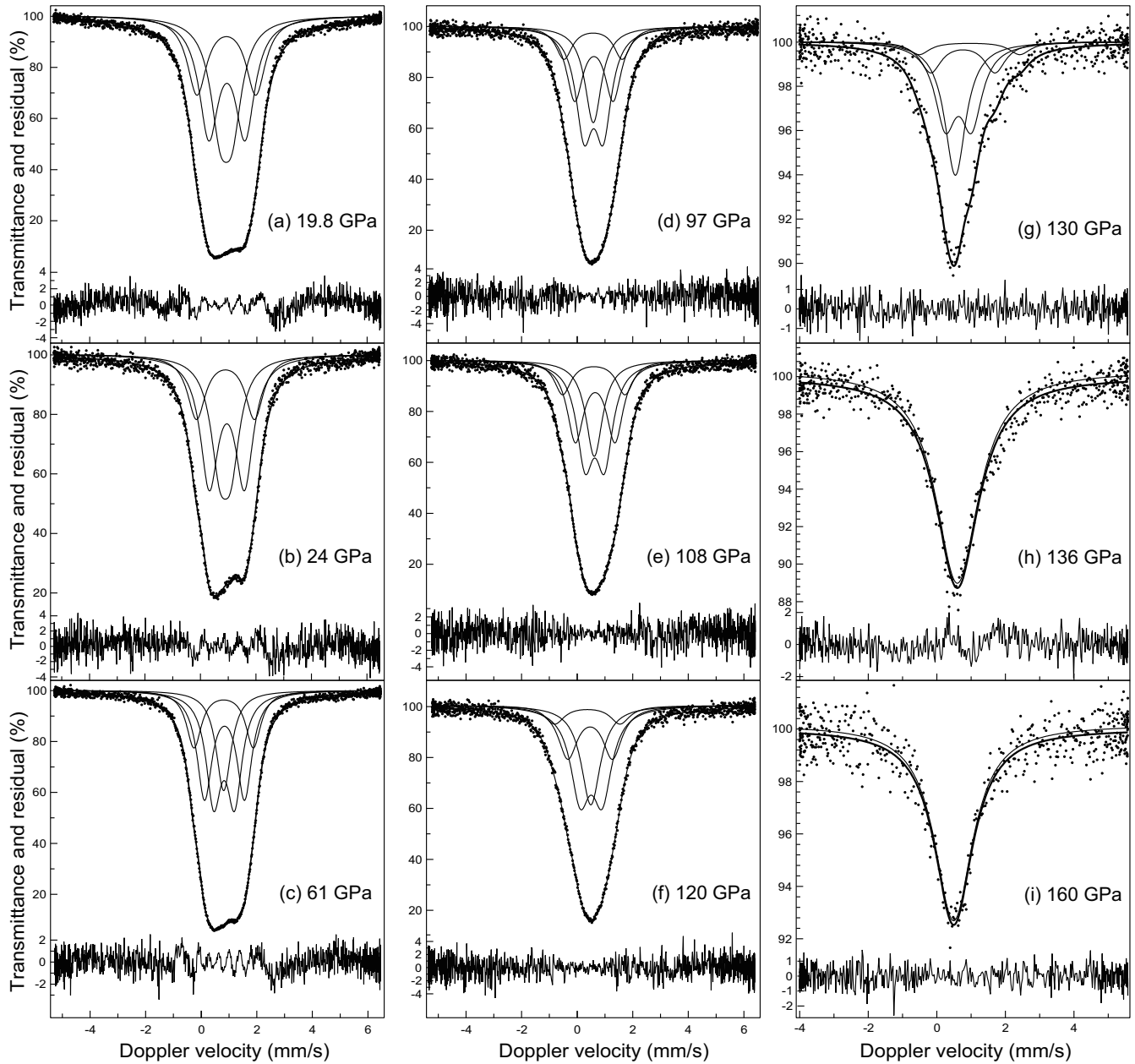


FIG. 4. Mössbauer spectra of $(\text{Mg}_{0.6}\text{Fe}^{2+}_{0.4})$ -ferropericlaite measured at room temperature. The residual is shown below for each spectrum. The doublets and singlet are least-square fits to the experimental data assuming quadrupole split components with different intensities. (a) and (b) Spectra fitted with three doublets. (c)–(g) Spectra fitted with three doublets and one singlet. (h) and (i) Spectra fitted with one singlet.

increasing pressure up to 120 GPa (Fig. 5). The IS values of the singlet also decrease with increasing pressure from 61 to 120 GPa, but those at 130, 136, and 160 GPa show similar values in a range between 0.49 and 0.59 mm/s.

In contrast to the result for $(\text{Mg}_{0.8}\text{Fe}_{0.2})\text{O}$ -ferropericlaite reported by Kantor *et al.* [7], indicating a strong non-monotonous pressure dependence of the QS (the increase of QS up to about 36–37 GPa and decrease at higher pressures), the systematic variation of QS of three doublets with increasing pressure from 19.8 to 120 GPa is not observed (Table I, Fig. 5). At pressures >120 GPa, the QS tends to increase with increasing pressure, which may be due to changes in the

distortion of the Fe^{2+}O_6 octahedra by transition of HS Fe^{2+} to LS Fe^{2+} .

As shown in Table I and Fig. 5, the sum of the area ratios of HS Fe^{2+} doublets, indicating the relative quantity of HS Fe^{2+} , gradually decreases with increasing pressure from 24.0 to 108 GPa at ambient temperature, while that of the LS Fe^{2+} singlet accordingly increases with a rather small gradient of the change. However, the area ratios of the doublets and singlet change abruptly under pressure conditions from 108 to 130 GPa. This change in the area ratios of the doublets and singlet is due to the progress of the spin transition of Fe^{2+} from HS to LS with increasing pressure.

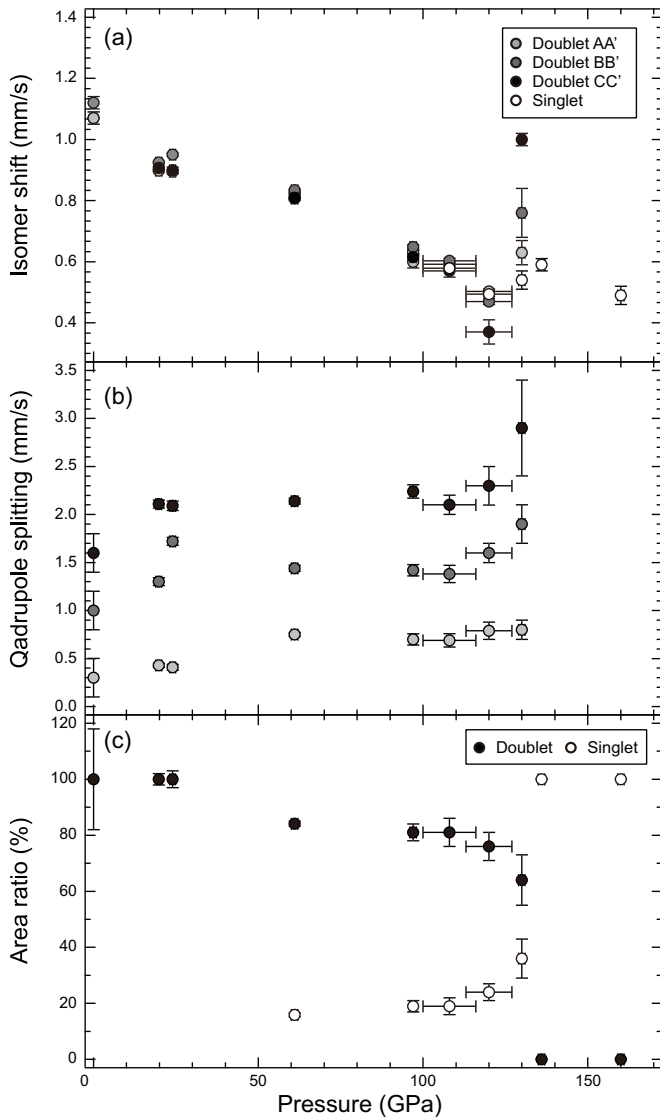


FIG. 5. Pressure dependence of (a) the isomer shift of the doublets and the singlet, (b) the quadrupole splitting of doublet, and (c) the area ratio of the doublets (closed circles) and the singlet (open circles). The isomer shift and quadrupole splitting were calculated from the doublets.

IV. DISCUSSION

A. Structural transition of $(\text{Mg}_{0.6}\text{Fe}_{0.4})\text{O}$ -ferropericlase at high pressure

According to the published studies, the structural transition of wüstite and ferropericlase with a high FeO content takes place at ~ 9 – 20 GPa [3,16–19], and the transition pressure increases with decreasing FeO contents. However, the structural transition pressure of ferropericlase with lower FeO content becomes unclear depending on the wüstite component. As mentioned in the Results section, $(\text{Mg}_{0.6}\text{Fe}_{0.4})\text{O}$ -ferropericlase has a B1 structure up to 160 GPa. Thus, the results of this paper and previous studies [35,47] suggest that the structural transition of $(\text{Mg}_{0.6}\text{Fe}_{0.4})\text{O}$ -ferropericlase does not take place at pressures in the lower mantle condition at room temperature and that the cubic B1 structure is stable.

The change of the cell volume with respect to the pressure gives us further information on the structural transition. At pressures >120 GPa, LS Fe^{2+} increases significantly, which causes the decrement of the cell volume. The gradient of the cell volume against pressure changes at ~ 130 GPa. Since all Fe^{2+} ions in the $(\text{Mg}_{0.6}\text{Fe}_{0.4})\text{O}$ -ferropericlase are in a LS state at pressures >136 GPa, the decrease of the cell volume at pressures of up to 160 GPa is attributed to the pressure effect. This result coincides with the result reported by Fei *et al.* [47], showing the volume change at ~ 120 – 140 GPa (Fig. 3).

B. Spin crossover region in $(\text{Mg}_{0.6}\text{Fe}_{0.4})\text{O}$ -ferropericlase

In this paper, we found a LS Fe^{2+} singlet in the Mössbauer spectrum measured at 61 GPa. This result suggests that the starting pressure of the spin crossover in $(\text{Mg}_{0.6}\text{Fe}_{0.4})\text{O}$ -ferropericlase at ambient temperature is located at 61 GPa. Solomatova *et al.* [35] indicated the spin crossover pressure range for the $(\text{Mg}_{0.52}\text{Fe}_{0.48})\text{O}$ to be from 45 to 84.5 GPa. Therefore, the starting pressures of the spin crossover region in both ferropericlases are similar to each other.

At pressures up to 120 GPa, both HS Fe^{2+} doublets and a LS Fe^{2+} singlet exist in the Mössbauer spectra, and at >136 GPa, the HS Fe^{2+} doublets disappear, and only the LS Fe^{2+} singlet is a component of the spectra. Moreover, the IS values of the HS Fe^{2+} doublets decrease with increasing pressure up to 120 GPa, and the IS value of the LS Fe^{2+} singlet decreases with increasing pressure at pressures >136 GPa. Therefore, it is concluded that the spin crossover of Fe^{2+} from the HS to the LS state in ferropericlase is completed at a pressure between 130 and 136 GPa.

In addition, Solomatova *et al.* [35] cautioned that reported spin transition pressures strongly depend on the pressure medium, pressure scale, other environmental conditions, and the criteria for assigning a particular pressure to the transition. The spin crossover of ferropericlase, magnesiowüstite, and wüstite (Fig. 6) has been reported as follows: spin crossover occurs at 90 to 140 GPa for $\text{Fe}_{0.94}\text{O}$ -wüstite [12], at 91 to 203 GPa at 300 K for $\text{Fe}_{0.96}\text{O}$ -wüstite [15], at 44 to 84 GPa for $(\text{Mg}_{0.52}\text{Fe}_{0.48})\text{O}$ -ferropericlase [35], at 52 to 70 GPa for $(\text{Mg}_{0.75}\text{Fe}_{0.25})\text{O}$ -ferropericlase [31], and at 50 to 100 GPa for $(\text{Mg}_{0.8}\text{Fe}_{0.2})\text{O}$ -ferropericlase [7]. These published data indicate that the spin crossover pressure region of wüstite occurs at a higher pressure than that of ferropericlase. As mentioned above, the starting pressure at 61 GPa for the spin crossover of $(\text{Mg}_{0.6}\text{Fe}_{0.4})\text{O}$ -ferropericlase in this paper is like that for ferropericlase reported by Solomatova *et al.* [35]. Despite the critical opinion by Solomatova *et al.* [35], the published data suggest that the pressure range of the spin crossover for ferropericlase depends on the FeO content (Fig. 6). Our result for the spin crossover pressure also lies on the increasing trend of the spin crossover pressure with FeO content. It is noted that the uppermost pressure of the spin crossover range in this paper between 120 and 136 GPa is higher than published data for other ferropericlases.

The existence of spin crossover of Fe in ferropericlase under lower mantle conditions has been suggested by some authors [51], and the LS Fe^{2+} increases in magma under lower mantle conditions [52,53], which could cause the ultra-low velocity zone (ULVZ) at the bottom of the lower mantle.

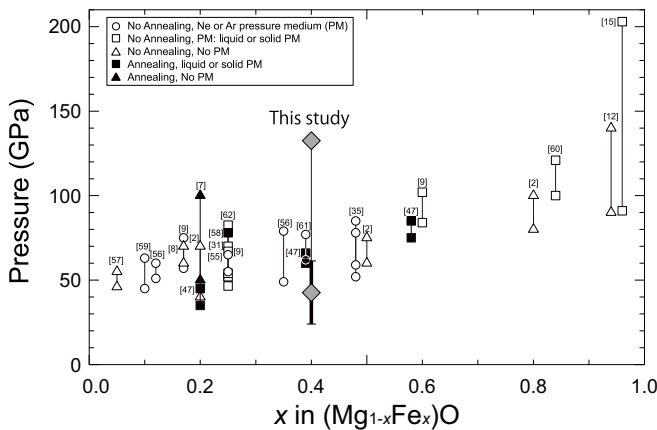


FIG. 6. The relationship between the wüstite component and the spin crossover region. The results of this paper are indicated by large diamond symbols. Symbols are as follows: open circle: experiments with gas pressure medium and no annealing before measurements [2,12,57], open square: experiments with liquid or solid pressure medium and no annealing before measurements, open triangle: experiments with no pressure medium and no annealing before measurements, closed square: experiments with liquid or solid pressure medium and annealing before measurements, closed triangle: experiments with no pressure medium and annealing before measurements. NaCl [2,9,47,58], KCl (this paper) [15,31,58], KBr (this paper), heavy mineral oil [62], and boron epoxy [60] are used as solid or liquid pressure media. Ne [9,35,54,55,59,61] and Ar [55,56] are also used as gas pressure media.

However, this paper revealed that HS and LS Fe^{2+} coexist in ferropericlase at the bottom of the lower mantle at ambient temperature since the temperature broadens the pressure

interval of the spin crossover and the coexistence of HS and LS Fe^{2+} is expected, even at the bottom of the lower mantle. Therefore, the spin transition of Fe may not significantly affect the formation processes of the ULVZ at the base of the lower mantle.

V. CONCLUSIONS

The structural transition under high pressure and the Fe^{2+} spin crossover pressure region in a synthetic $(\text{Mg}_{0.6}\text{Fe}_{0.4})\text{O}$ -ferropericlase were investigated using synchrotron Mössbauer spectroscopy and the synchrotron XRD method in the pressure range from 19.8 to 160 GPa. It was clarified that the cubic B1 structure of the $(\text{Mg}_{0.6}\text{Fe}_{0.4})\text{O}$ -ferropericlase remains at least up to 160 GPa. The spin crossover in the $(\text{Mg}_{0.6}\text{Fe}_{0.4})\text{O}$ -ferropericlase starts at ~ 61 GPa and is complete at 136 GPa at ambient temperature, implying that both HS and LS Fe^{2+} coexist at the pressure conditions from the upper part of the lower mantle to the mantle-core boundary.

ACKNOWLEDGMENTS

This paper was supported by Grant-in-Aid for Scientific Research on Priority Areas JP22000002 from the Ministry of Education, Culture, Sports, Science and Technology (MEXT) to E.O. and a Grant-in-Aid for Scientific Research(S) JP15H05748 from the Japan Society for the Promotion of Science (JSPS) to E.O. The synchrotron radiation experiments were performed at the SPring-8 facility with the approval of the Japan Synchrotron Radiation Research Institute (Proposal No. 2013B3517, 2014A0104) and the Japan Atomic Energy Agency (Proposal No. 2013B-E07).

- [1] S. D. Jacobsen, J. F. Lin, R. J. Angel, G. Shen, V. B. Prakapenka, P. Dera, H. K. Mao, and R. J. Hemley, *J. Synchrotron Rad.* **12**, 577 (2005).
- [2] S. Speziale, A. Milner, V. E. Lee, S. M. Clark, M. P. Pasternak, and R. Jeanloz, *Proc. Natl. Acad. Sci. U.S.A.* **102**, 17918 (2005).
- [3] S. Speziale, V. E. Lee, S. M. Clark, J. F. Lin, M. P. Pasternak, and R. Jeanloz, *J. Geophys. Res. Solid Earth* **112**, B10212 (2007).
- [4] A. P. Kantor, S. D. Jacobsen, I. Y. Kantor, L. S. Dubrovinsky, C. A. McCammon, H. J. Reichmann, and I. N. Goncharenko, *Phys. Rev. Lett.* **93**, 215502 (2004).
- [5] I. Y. Kantor, C. A. McCammon, and L. S. Dubrovinsky, *J. Alloy. Compd.* **376**, 5 (2004).
- [6] I. Y. Kantor, L. S. Dubrovinsky, and C. A. McCammon, *Phys. Rev. B* **73**, 100101(R) (2006).
- [7] I. Kantor, L. Dubrovinsky, C. McCammon, A. Kantor, S. Pascarelli, G. Aquilanti, W. Crichton, M. Mattesini, R. Ahuja, J. Almeida, and V. Ursov, *Phys. Chem. Miner.* **33**, 35 (2006).
- [8] J. Badro, G. Fiquet, F. Guyot, J. P. Fuffe, V. V. Struzhkin, G. Vankó, and G. Monaco, *Science* **300**, 789 (2003).
- [9] J. F. Lin, V. V. Struzhkin, S. D. Jacobsen, M. Y. Hu, P. Chow, J. Kung, H. Liu, H. K. Mao, and R. J. Hemley, *Nature* **436**, 377 (2005).
- [10] J. F. Lin, G. Vankó, S. D. Jacobsen, V. Iota, V. V. Struzhkin, V. B. Prakapenka, A. Kuznetsov, and C. S. Yoo, *Science* **317**, 1740 (2007).
- [11] C. A. McCammon and D. C. Price, *Phys. Chem. Miner.* **11**, 250 (1985).
- [12] M. P. Pasternak, R. D. Taylor, R. Jeanloz, X. Li, J. H. Nguyen, and C. A. McCammon, *Phys. Rev. Lett.* **79**, 5046 (1997).
- [13] H. Ozawa, K. Hirose, K. Ohta, H. Ishii, N. Hiraoka, Y. Ohishi, and Y. Seto, *Phys. Rev. B* **84**, 134417 (2011).
- [14] K. Ohta, K. Hirose, K. Shimizu, and Y. Ohishi, *Phys. Rev. B* **82**, 174120 (2010).
- [15] M. Hamada, S. Kamada, E. Ohtani, T. Mitsui, R. Masuda, T. Sakamaki, N. Suzuki, F. Maeda, and M. Akasaka, *Phys. Rev. B* **93**, 155165 (2016).
- [16] G. T. Zou, H. K. Mao, P. M. Bell, and D. Virgo, *Year Book Carnegie Inst. Washington* **79**, 374 (1980).
- [17] T. Yagi, T. Suzuki, and S. Akimoto, *J. Geophys. Res. Solid Earth* **90**, 8784 (1985).
- [18] H. K. Mao, J. Shu, Y. Fei, J. Hu, and R. J. Hemley, *Phys. Earth Planet. Inter.* **96**, 135 (1996).
- [19] J. Shu, H. K. Mao, J. Fu, Y. Fei, and R. J. Hemley, *Neues. Jahrb. Miner. Abh.* **172**, 309 (1998).
- [20] I. Kantor, Ph.D. thesis, Universität Bayreuth, Bayern, Germany, (2007).

- [21] J. F. Lin, D. L. Heinz, H. K. Mao, R. J. Hemley, J. M. Devine, J. Li, and G. Shen, *Proc. Natl. Acad. Sci. U.S.A.* **100**, 4405 (2003).
- [22] Y. Fei and H. K. Mao, *Science* **266**, 1678 (1994).
- [23] D. M. Sherman and H. J. F. Jansen, *Geophys. Res. Lett.* **22**, 1001 (1995).
- [24] T. Kondo, E. Ohtani, N. Hirao, T. Yagi, and T. Kikegawa, *Phys. Earth Planet. Inter.* **143–144**, 201 (2004).
- [25] M. Murakami, K. Hirose, S. Ono, T. Tsuchiya, M. Isshiki, and T. Watanuki, *Phys. Earth Planet. Inter.* **146**, 273 (2004).
- [26] R. A. Fischer, A. J. Campbell, G. A. Shofner, O. T. Lord, P. Dera, and V. B. Prakapenka, *Earth Planet. Sci. Lett.* **304**, 496 (2011).
- [27] P. Kaercher, S. Speziale, L. Miyagi, W. Kanitpanyacharoen, and H.-R. Wnk, *Phys. Chem. Miner.* **39**, 613 (2012).
- [28] J. S. Smart and S. Greenwald, *Phys. Rev.* **82**, 113 (1951).
- [29] V. V. Struzhkin, H. K. Mao, J. Hu, M. Schwoerer-Böhning, J. Shu, R. J. Hemley, W. Sturhahn, M. Y. Hu, E. E. Alp, P. Eng, and G. Shen, *Phys. Rev. Lett.* **87**, 255501 (2001).
- [30] J. Badro, V. V. Struzhkin, J. Shu, R. J. Hemley, H. K. Mao, C. C. Kao, J. P. Rueff, and G. Shen, *Phys. Rev. Lett.* **83**, 4101 (1999).
- [31] J. F. Lin, A. G. Gavriiliuk, V. V. Struzhkin, S. D. Jacobsen, W. Sturhahn, M. Y. Hu, P. Chow, and C. S. Yoo, *Phys. Rev. B* **73**, 113107 (2006).
- [32] T. Tsuchiya, R. M. Wentzcovitch, C. R. S. da Silva, and S. de Gironcoli, *Phys. Rev. Lett.* **96**, 198501 (2006).
- [33] K. Persson, A. Bengtson, G. Ceder, and D. Morgan, *Geophys. Res. Lett.* **33**, L16306 (2006).
- [34] Y. Fei, H. K. Mao, J. Shu, and J. Hu, *Phys. Chem. Miner.* **18**, 416 (1992).
- [35] N. V. Solomatova, J. M. Jackson, W. Sturhahn, J. K. Wicks, J. Zhao, T. S. Toellner, B. Kalkan, and W. M. Steinhardt, *Am. Miner.* **101**, 1084 (2016).
- [36] R. H. Nafziger, G. C. Ulmer, and E. Woermann, *Gaseous Buffering for the Control of Oxygen Fugacity at One Atmosphere* (Springer, Berlin, 1971), p. 9.
- [37] Y. Seto, D. Nishio-Hamane, T. Nagai, and N. Sata, *Review of High Pressure Science and Technology* **20**, 269 (2010), (in Japanese).
- [38] Y. Seto, *Review of High Pressure Science and Technology* **22**, 144 (2012), (in Japanese).
- [39] M. Rosenhauer, H. K. Mao, and E. Woermann, *Carnegie Institution Year Books* **75**, 513 (1976).
- [40] A. Dewaele, F. Datchi, P. Loubeyre, and M. Mezouar, *Phys. Rev. B* **77**, 094106 (2008).
- [41] Y. Akahama, and H. Kawamura, *J. Appl. Phys.* **96**, 3748 (2004).
- [42] Y. Ohishi, N. Hirao, N. Sata, Hirose K, and M. Takata, *High Pressure Res.* **28**, 163 (2008).
- [43] T. Mitsui, N. Hirao, Y. Ohishi, R. Masuda, Y. Nakamura, H. Enoki, K. Sasaki, and M. Seto, *J. Synchrotron Rad.* **16**, 723 (2009).
- [44] N. Hirao, S. I. Kawaguchi, K. Hirose, K. Shimizu, E. Ohtani, and Y. Ohishi, *Matter. Radiat. Extremes* **5**, 018403 (2020).
- [45] C. Prescher, C. A. McCammon, and L. S. Dubrovinsky, *J. Appl. Crystallogr.* **45**, 329 (2012).
- [46] K. Takemura, *Rev. High Pres. Sci. Tech.* **22**, 283 (2012).
- [47] Y. Fei, L. Zhang, A. Corgne, H. Watson, A. Ricolleau, Y. Meng, and V. Prakapenka, *Geophys. Res. Lett.* **34**, L17307 (2007).
- [48] E. Dowty and D. H. Lindsley, *Am. Miner.* **58**, 850 (1973).
- [49] F. Seifert, M. Czank, B. Simons, and W. Schmahl, *Phys. Chem. Miner.* **14**, 26 (1987).
- [50] M. Hamada and M. Akasaka, *Phys. Chem. Miner.* **40**, 259 (2013).
- [51] J. F. Lin, S. Speziale, Z. Mao, and H. Marquardt, *Rev. Geophys.* **51**, 244 (2013).
- [52] R. Nomura, H. Ozawa, S. Tateno, K. Hirose, J. Herlund, S. Muto, H. Ishii, and N. Hiraoka, *Nature* **473**, 199 (2011).
- [53] S. Fu, J. Yang, Y. Zhang, J. Liu, E. Greenberg, V. B. Prakapenka, T. Okuchi, and J. F. Lin, *Earth Planet. Sci. Lett.* **503**, 1 (2018).
- [54] B. Chen, J. M. Jackson, W. Sturhahn, D. Zhang, J. Zhao, J. K. Wicks, and C. A. Murphy, *J. Geophys. Res.* **117**, B08208 (2012).
- [55] A. F. Goncharov, V. V. Struzhkin, and S. D. Jacobsen, *Science* **312**, 1205 (2006).
- [56] H. Keppler, I. Y. Kantor, and L. S. Dubrovinsky, *Am. Miner.* **92**, 433 (2007).
- [57] J. F. Lin, V. V. Struzhkin, A. G. Gavriiliuk, and I. Lyubutin, *Phys. Rev. B* **75**, 177102 (2007).
- [58] Z. Mao, J. F. Lin, J. Liu, and V. B. Prakapenka, *Geophys. Res. Lett.* **38**, L23308 (2011).
- [59] H. Marquardt, S. Speziale, H. J. Reichmann, D. J. Frost, and F. R. Schilling, *Earth Planet. Sci. Lett.* **287**, 345 (2009).
- [60] J. K. Wicks, J. M. Jackson, and W. Sturhahn, *Geophys. Res. Lett.* **37**, L15304 (2010).
- [61] K. K. Zhuravely, J. M. Jackson, A. S. Wolf, J. K. Wicks, J. Yan, and S. M. Clark, *Phys. Chem. Miner.* **37**, 465 (2010).
- [62] J. F. Lin, Z. Mao, I. Jarrige, Y. Xiao, P. Chow, T. Okuchi, N. Hiraoka, and S. D. Jacobsen, *Am. Miner.* **95**, 1125 (2010).